Diagnostic efficiency of intravoxel incoherent motion-based virtual magnetic resonance elastography in pulmonary neoplasms

Shuo Zhang[1†], Yonghao Du[1†], Ting Liang[1], Xuyin Zhang[1], Yinxia Guo[1], Jian Yang[1], Xianjun Li[1*] and Gang Niu[1*]

Abstract

Background The aim of the study were as below. (1) To investigate the feasibility of intravoxel incoherent motion (IVIM)-based virtual magnetic resonance elastography (vMRE) to provide quantitative estimates of tissue stiffness in pulmonary neoplasms. (2) To verify the diagnostic performance of shifted apparent diffusion coefficient (sADC) and reconstructed virtual stiffness values in distinguishing neoplasm nature.

Methods This study enrolled 59 patients (37 males, 22 females) with one pulmonary neoplasm who underwent computed tomography-guided percutaneous transthoracic needle biopsy (PTNB) with pathological diagnosis (26 adenocarcinoma, 10 squamous cell carcinoma, 3 small cell carcinoma, 4 tuberculosis and 16 non-specific benign; mean age, 60.81 ± 9.80 years). IVIM was performed on a 3 T magnetic resonance imaging scanner before biopsy. sADC and virtual shear stiffness maps reflecting lesion stiffness were reconstructed. sADC and virtual stiffness values of neoplasm were extracted, and the diagnostic performance of vMRE in distinguishing benign and malignant and detailed pathological type were explored.

Results Compared to benign neoplasms, malignant ones had a significantly lower sADC and a higher virtual stiffness value ($P < 0.001$). Subsequent subtype analyses showed that the sADC values of adenocarcinoma and squamous cell carcinoma groups were significantly lower than non-specific benign group ($P = 0.013$ and 0.001, respectively). Additionally, virtual stiffness values of the adenocarcinoma and squamous cell carcinoma subtypes were significantly higher than non-specific benign group ($P = 0.008$ and 0.001, respectively). However, no significant correlation was found among other subtype groups.

Conclusions Non-invasive vMRE demonstrated diagnostic efficiency in differentiating the nature of pulmonary neoplasm. vMRE is promising as a new method for clinical diagnosis.

Keywords Intravoxel incoherent motion, Virtual magnetic resonance elastography, Stiffness, Shifted apparent diffusion coefficient, Pulmonary neoplasm

---

†Shuo Zhang and Yonghao Du contributed equally to this work.

*Correspondence:
Xianjun Li
xianj.li@mail.xjtu.edu.cn
Gang Niu
niugang369@mail.xjtu.edu.cn
[1]Department of Radiology, the First Affiliated Hospital of Xi'an Jiaotong University, 277 Yanta West Road, Yanta District, Xi'an 710061, P.R. China

Zhang *et al. Cancer Imaging*   (2024) 24:88

Page 2 of 8

Background

Lung cancer is the most common malignancy and the leading cause of cancer-related death worldwide [1, 2]. Accurate diagnosis of benign and malignant pulmonary neoplasm and identification of pathological type are crucial for clinical decision-making. Biopsy and radiological techniques with contrast administration are mostly necessary for establishing diagnosis, but both have contraindications and complications. Moreover, the diagnostic performance of conventional radiological methods needs to be improved. Due to the limitations of these existing tools, exploring non-invasive techniques with the potential of replacing invasive histopathologic analysis of pulmonary neoplasm remains urgent.

Stiffness is an intrinsic material property of the tissue. Increased tissue stiffness is the most tangible and best-recognized mechanical abnormality in tumors [3]. Magnetic resonance elastography (MRE) was developed to probe the mechanical properties of tissue and allow an estimation of the true viscoelasticity of various tissues and organs. However, due to the poor portability and limited availability of the appropriate magnetic resonance (MR) equipment, the clinical application of MRE has large limitations [4].

Intravoxel Incoherent Motion (IVIM)-based virtual MRE (vMRE) is a novel method with potential application for the non-invasive assessment of tissue stiffness and without the limitation of specialized hardware and expertise of traditional MRE [5]. This method was first proposed by Le Bihan et al. in the evaluation of liver fibrosis, and it was subsequently verified in a small (n=15) [5] and a larger patient cohort (n=74) [6]. These previous studies reveal a strong correlation between tissue water diffusivity and tissue elasticity in the liver. In short, diffusion MR imaging, through a calibration of shifted apparent diffusion coefficient (sADC) values with standard MRE, can be converted quantitatively into shear modulus to provide tissue stiffness information, requiring only two b values [5].

As a non-invasive method that relies on widely available magnetic resonance imaging (MRI) sequences with high image resolution and short acquisition time, the application of vMRE has been extended to other diseases of the liver (e.g., hepatocellular carcinoma, liver metastases [7], non-alcoholic fatty liver disease [8]) and brain (e.g., pituitary adenoma [9] and meningiomas [10]). For other organs and diseases, tissue elastic properties and tissue microstructure should be tightly related, similar to liver tissue. Therefore, we hypothesized that vMRE could provide information for judging pulmonary neoplasms. This vMRE application could make up for the shortcomings of conventional radiological methods by introducing elastic parameters to improve diagnostic efficiency. The aim of this study was to explore the capability of vMRE in the characterization of pulmonary neoplasms through quantitative sADC and virtual stiffness values. To our knowledge, the method has not previously been used in pulmonary neoplasm evaluation.

Methods

Study participants

Consecutive pulmonary neoplasm patients who underwent a computed tomography (CT)-guided percutaneous lung biopsy between April 2018 and March 2020 were enrolled in our study. The inclusion criteria were as follows: (1) CT-confirmed primary pulmonary neoplasm; (2) lesion diameter≥3.0 cm; (3) each neoplasm had an exact pathological diagnosis; (4) patient free from any comorbidities or previous cancers. The exclusion criteria were as follows: (1) the boundary between the lesion and adjacent structures was unclear; (2) the images were blurred with obvious artifacts; (3) patient had already received antitumor therapy prior to IVIM examination; (4) pulmonary metastasis (primary tumors outside the chest).

MR imaging protocol

MRI was performed using a 3 T Signa HDXT (General Electric, Milwaukee, WI, USA) with an eight-channel body phased-array coil for signal reception. The scanning was stopped immediately once the participants felt uncomfortable. IVIM images were collected with the following b values: 0, 10, 15, 20, 25, 50, 80, 150, 300, 500 and 800 s/mm^2. All MRI sequences and parameters are listed in Table 1.

vMRE stiffness quantification

After scanning, sADC and virtual stiffness values were calculated by two key b values (low key b value, LKb, and high key b value, HKb) to estimate the shear modulus of pulmonary neoplasm. The quantification is summarized below (Eqs. 1 and 2) and described in detail by Le Bihan et al. [5].

$$\text{sADC}\ (\text{s/mm}^2) = \ln\left(S_{\text{LKb}}/S_{\text{HKb}}\right)/\left(\text{HKb} - \text{LKb}\right)\ \textbf{(1)}$$

Table 1 3.0-T MR imaging sequences and parameters

Parameter	T2-2D FSE	T1-2D FIESTA	IVIM
Respiration pattern	Breath-hold	Breath-hold	Breath-hold
Plane	Axial	Axial	Axial
Repetition time (ms)	8000	3.2	9000
Echo time (ms)	95.1	1.1	65.4
Matrix	512×512	512×512	512×512
Section thickness/slice spacing (mm)	5/0	5/0	4/0
Field of view (mm)	400	350	400

Note FSE: fast spin echo; FIESTA: fast imaging employing steady-state acquisition

$$\text{virtual stiffness} \, (\text{kPa}) = \alpha \cdot \ln \, (S_{low}/S_{high}) + \beta \qquad (2)$$

S_{LKb} and S_{HKb} represent intensities of the signals acquired at the low and high key b values, which were S_{low} (b value=150 s/mm^2) and S_{high} (b value=800 s/mm^2) in our study, respectively. The scaling (α) and the shift (β) factors were separately set to -9.8 and 14, respectively, according to the previous calibration studies.

Image analysis

Two radiologists, each with more than five years of experience in diagnosing chest images, drew the regions of interest (ROI) independently on sADC and shear stiffness maps. The ROIs were placed on three contiguous axial slices, in which the tumors had maximum diameters, and to avoid necrotic, bleeding, or inhomogeneous areas. The average value was recorded from these ROIs. Both radiologists were blinded to the patients' clinical history and histopathological diagnosis.

The quantification of sADC and virtual stiffness were performed off-line using MATLAB R2016a (Mathworks, Natick, Massachusetts, USA).

Statistical analysis

After assessing the normal distribution of sADC and virtual stiffness values with the Kolmogorov-Smirnov test, Mann-Whitney U test was used to evaluate differences between benign and malignant pulmonary neoplasm groups. Categorical variables are shown as the number and were compared using the chi-squared test. One-way analysis of variance (ANOVA) was performed to calculate the differential values of each pathological pattern in the malignant groups. The receiver operating characteristic (ROC) curve was used to assess the discrimination capability of the pulmonary neoplasm property. The intra- and inter-observer agreement was determined using intraclass correlation coefficients (ICC) with 95% confidence intervals, where the two-sided random ICC model was used to determine the consistency of the agreement. Statistical analyses were all performed using SPSS software (version 18.0, IBM, Chicago, IL). Statistical significance was accepted as a two-sided P value<0.05.

Results

Characteristics of the study participants

We recruited 68 individuals for our study. Seven patients were excluded because of artifacts on IVIM images (mainly from respiratory or heart motion). After 2 years follow-up, two non-specific benign cases were excluded because the final diagnosis were malignant. We finally enrolled 59 participants (36 males, 23 females; mean age at diagnosis: 60.81±9.80 years), each with one pulmonary neoplasm for further assessment. The enrollment procedure is presented in Fig. 1. These patients were divided
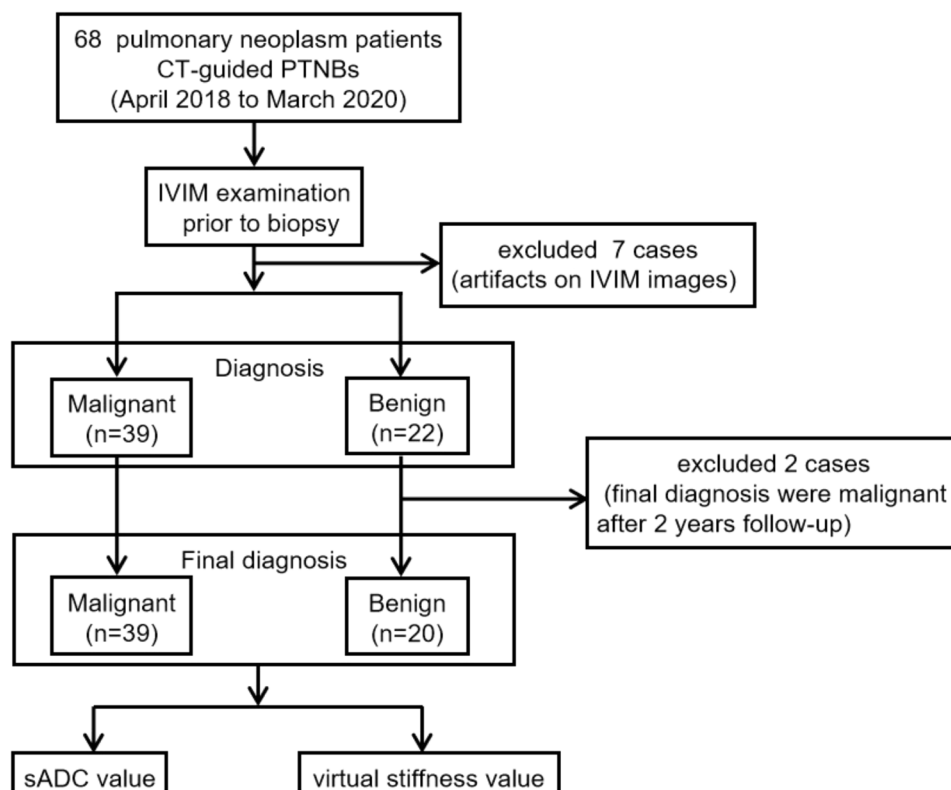

Fig. 1 Flow chart of the enrollment process

Zhang *et al. Cancer Imaging*   (2024) 24:88

Page 4 of 8

Table 2 Clinical characteristics of patients with pulmonary neoplasm

Characteristics	Malignant $n=39$	Benign $n=20$	P
Age (years)	61.03 ± 10.23	59.94 ± 9.41	0.820
Male/Female	24/15	13/7	0.796
Lesion diameter (cm)	4.93 ± 1.88	4.12 ± 1.11	0.010*
Location			0.073
Upper/Middle lobe	27	9	
Lower lobe	12	11	

Note *P value<0.05 indicates statistical significance. Date are shown as Mean±SD. Continuous variables were compared using the Mann-Whitney U test. Categorical variables are shown as the number and were compared using the chi-squared test

Table 3 Intra- and inter-observer reproducibility in Assessment of sADC and virtual stiffness

	ICC (95% CI)	
	Intra-observer	Inter-observer
sADC(s/mm^2)	0.956 (0.927–0.974)	0.864 (0.782–0.917)
virtual stiffness (kPa)	0.941 (0.903–0.964)	0.887 (0.826–0.928)

Note ICC, intra-class correlation coefficient. 95% CI, 95% confidence interva

Table 4 sADC and virtual stiffness of Benign and Malignant neoplasms

	sADC ($\times 10^{-4}$, b=200,800 s/mm^2) Mean±SD (95% C.I.)	virtual stiffness (kPa) Mean±SD (95% C.I.)
Malignant($n=39$)	5.78 ± 2.03 (5.12–6.43)	9.53 ± 1.77 (8.96–10.11)
Benign ($n=20$)	8.47 ± 1.99 (7.54–9.40)	7.27 ± 1.60 (6.52–8.01)
P value	<0.001***	<0.001***

Note *P value<0.05 indicates statistical significance; ***P<0.001
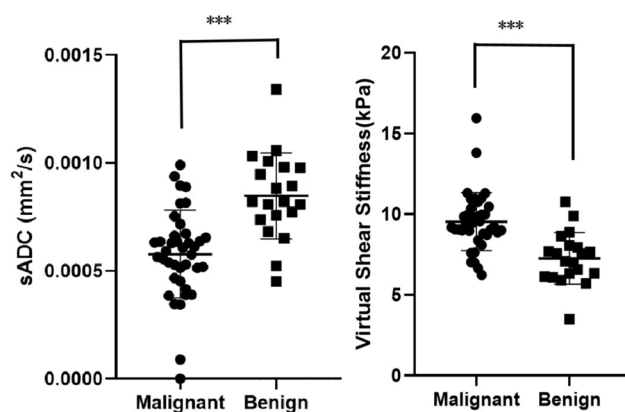
Fig. 2 Comparison of sADC and virtual stiffness values between benign and malignant groups. sADC value in malignant group was significantly lower than benign group (P<0.001), while virtual stiffness value in malignant group was significantly higher than benign group (P<0.001)

into two groups based on their final histopathological diagnosis. The malignant group (39/59) included patients with adenocarcinoma, squamous cell carcinoma and small-cell carcinoma, whereas the benign group (20/59) included patients with tuberculosis and non-specific

benign. Table 2 lists the clinical characteristics of the enrolled patients.

Intra- and inter-observer reproducibility agreement

The intra- and inter-observer reproducibility for measurement of sADC and virtual stiffness values are presented in Table 3. Good intra- and inter-observer reproducibility were obtained, with ICC values in the range of 0.864–0.956.

sADC and virtual stiffness values were significantly different in malignant and benign pulmonary neoplasms

After scanning, sADC and shear stiffness maps were obtained. Next, we compared sADC and virtual stiffness values of each pulmonary neoplasm to determine whether there was any difference between malignant and benign groups. As shown in Table 4; Fig. 2, the mean value of sADC in the malignant group was significantly lower than that in the benign group ($5.78 \times 10^{-4} \pm 2.03 \times 10^{-4}$ s/mm^2 versus $8.47 \times 10^{-4} \pm 1.99 \times 10^{-4}$ s/mm^2, P<0.001). As for virtual stiffness, a higher value was observed in the malignant group than in the benign group (9.53 ± 1.77 kPa versus 7.27 ± 1.60 kPa, P<0.001). Examples of T1-weighted (T1W) fast imaging employing steady-state acquisition (FIESTA) axial images and fat saturated T2-weighted (T2W) fast spin echo (FSE) axial images together with sADC maps in benign and malignant neoplasms are presented in Fig. 3. An ROC curve was drawn to assess the discrimination capability of pulmonary neoplasm property. The areas under the curve of sADC and virtual stiffness values for distinguishing pulmonary neoplasm nature were 0.840 and 0.847, respectively. The sensitivity and specificity in differentiating malignant from benign neoplasms were 79.5% and 85.0% for sADC versus 84.6% and 80.0% for virtual stiffness values (Fig. 4). The cut-off value of sADC was 6.78×10^{-4} s/mm^2, while that for the virtual stiffness value was 8.08 kPa. These results indicate that the sADC and virtual stiffness values possess the potential to predict pulmonary neoplasm properties.

Subtype analyses of sADC and virtual stiffness values

We subsequently compared sADC and virtual stiffness values among each pathological pattern. The data showed that the sADC values of the adenocarcinoma and squamous cell carcinoma groups were lower than the non-specific benign group, while virtual stiffness values were higher in the two subtypes of malignant pulmonary neoplasm. As shown in Table 5; Fig. 5, we found significantly higher sADC values in the non-specific benign group compared to the adenocarcinoma and squamous cell carcinoma groups (P=0.013 and 0.001, respectively). The mean virtual stiffness values among the three groups also reached statistical significance, with P values of 0.008
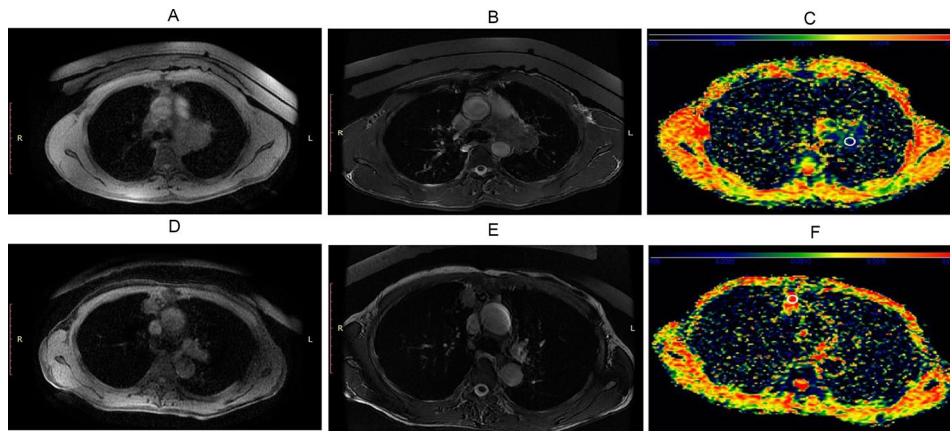
Fig. 3 T1-2D FIESTA and T2-2D FSE images together with sADC maps in benign and malignant neoplasms. The adenocarcinoma in the upper lobe of the left lung presented signs of lower sADC and higher virtual stiffness values in sADC map (A-C). The inflammatory nodule in the upper lobe of the right lung displayed signs of higher sADC and lower virtual stiffness values in sADC map (D-F). Regions of interests (ROIs) on C and F (white circle) were set to measure the sADC value of the two cases. FIESTA: fast imaging employing steady-state acquisition; FSE: fast spin echo
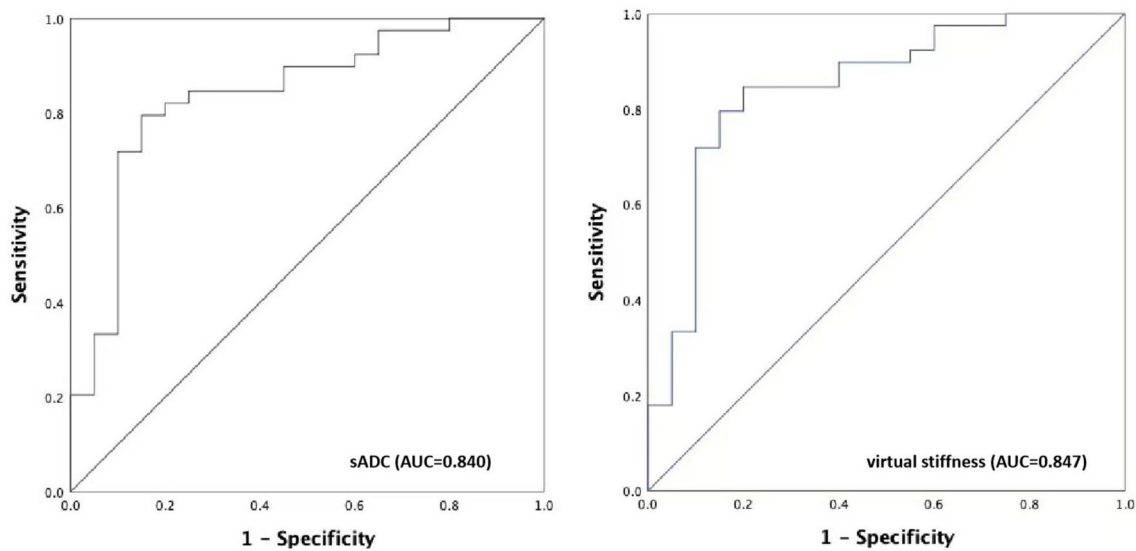

Fig. 4 Receiver operating characteristic (ROC) curves of sADC and virtual stiffness. The areas under the ROC curves of the sADC and virtual stiffness were 0.840 and 0.847, respectively. The sensitivity and specificity of sADC were 79.5% and 85.0%, and those of virtual stiffness were 84.6% and 80.0%, respectively

Table 5 Comparison of sADC and virtual stiffness values for detailed pathological type

	sADC (×10⁻⁴, b = 200,800 s/mm²) Mean ± SD (95% C.I.)	virtual stiffness (kPa) Mean ± SD (95% C.I.)
AC (*n* = 26)	6.28 ± 1.70 (5.60–6.97)	9.07 ± 1.33 (8.53–9.61)
SqCC (*n* = 10)	4.90 ± 1.97 (3.49–6.30)	10.21 ± 1.66 (9.03–11.40)
SCC (*n* = 3)	4.31 ± 3.73 (4.95–13.57)	11.27 ± 4.05 (1.20-21.34)
TB (*n* = 4)	7.93 ± 1.02 (6.31–9.54)	7.78 ± 0.79 (6.52–9.05)
Non-specific benign (*n* = 16)	8.60 ± 2.17 (7.45–9.76)	7.14 ± 1.74 (6.21–8.07)
P value	< 0.001***	< 0.001***
Post-Hoc Test *P* value	0.013* (AC vs. Non-specific benign) 0.001** (SqCC vs. Non-specific benign)	0.008** (AC vs. Non-specific benign) 0.001** (SqCC vs. Non-specific benign)

Note AC: Adenocarcinoma; SqCC: Squamous cell carcinoma; SCC: Small-cell carcinoma; TB: Tuberculosis

*P-value < 0.05 indicates statistical significance; **P < 0.01; ***P < 0.001

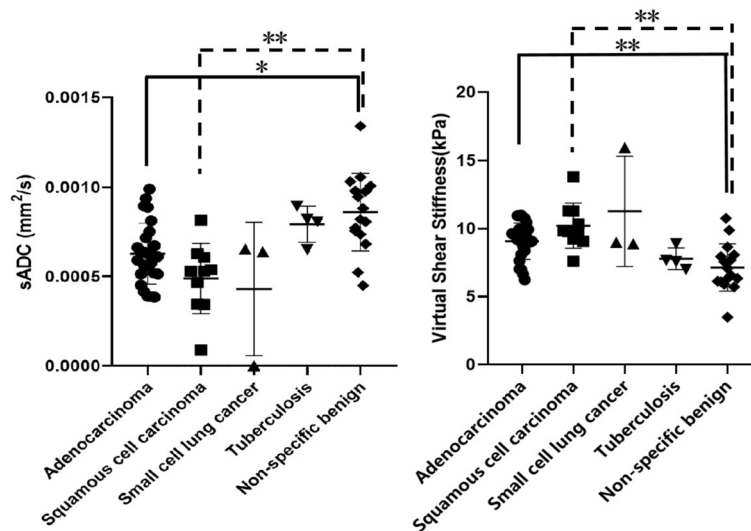Zhang *et al. Cancer Imaging*   (2024) 24:88

Page 6 of 8

Fig. 5 Comparison of sADC and virtual stiffness values for detailed pathological type. sADC value of adenocarcinoma and squamous cell carcinoma groups was lower than that of non-specific benign group ($P = 0.013$ and 0.001, respectively). Virtual stiffness value of the two malignant subtypes is higher than that of non-specific benign group ($P = 0.008$ and 0.001, respectively)

(adenocarcinoma versus non-specific benign) and 0.001 (squamous cell carcinoma versus non-specific benign), respectively. We also compared sADC and virtual stiffness values between malignant and tuberculosis groups. As shown in Supplementary Table, the differences in these two parameters between the two groups were statistically significant. Nevertheless, no significant difference was found among other pathological patterns.

Discussion

The non-invasive diagnostic vMRE method was first developed and used for liver fibrosis assessments, suggesting a strong correlation between liver tissue elastic properties as revealed with standard MRE, and tissue microstructure as shown with diffusion MR imaging [5]. This correlation was due to the elastic properties of tissues which are linked to the layout of elementary tissue components (i.e., cells, fibers, stroma) to which diffusion MR imaging was exquisitely sensitive [11]. Based on this relationship, vMRE was subsequently applied to hepatocellular carcinoma, liver metastases, non-alcoholic fatty liver disease, pituitary adenoma, and meningiomas, and was considered for potential expansion to the spleen (portal hypertension), breast, prostate (cancer), and brain (neurological disorders) [5]. In this study, vMRE for evaluation of pulmonary neoplasm was proposed to have the potential to indicate stiffness and distinguish property. We present the first study in which malignant neoplasms possessed significantly lower sADC and higher mean virtual stiffness values compared to benign neoplasms. Adenocarcinoma and squamous cell carcinoma were significantly stiffer than non-specific benign neoplasm.

In order to reduce the interference of non-diagnostic percutaneous transthoracic needle biopsy (PTNB) results to the data in this study, we conducted a two-year follow-up of each patient with a pathologically benign diagnosis. Ultimately, two patient were excluded, with a consistent occurrence rate of previous study [12].

A considerable number of studies have used diffusion-weighted imaging (DWI) and IVIM based methods to explore correlations between quantitative parameters, image characteristics, and pulmonary neoplasm. Nevertheless, there have been no deep learning or radiomics studies involving these functional sequences. A meta-analysis on the diagnostic performance of IVIM found that tissue diffusivity (D) value demonstrated the best diagnostic performance and highest post-test probability in the differential diagnosis of lung tumors, followed by the apparent diffusion coefficient (ADC), perfusion fraction (f), and pseudo-diffusivity (D*) values [13]. Other studies involved the differentiation, staging, and proliferation of lung cancer [14], the detection of mediastinal lymph node metastasis [15], the evaluation of lung cancer efficacy, and the prediction of antitumor drug response [16, 17]; all indicated that IVIM-DWI has the potential of comprehensive pulmonary neoplasm evaluation. One previous study reported a significant but moderate correlation of MR elastographic shear modulus with standard ADC and a significant but moderate correlation with the non-Gaussian diffusion index (NGD) [18]. However, the correlation between shear modulus and diffusivity was more prominent with the sADC in which non-Gaussian diffusion effects are incorporated over the ADC. Therefore, sADC is more sensitive to the tissue microstructure compared to ADC [5].

Zhang *et al. Cancer Imaging*   (2024) 24:88

Page 7 of 8

Most studies that have examined lung stiffness were limited to ultrasound elastography. Kuo et al. reported that transthoracic shear-wave ultrasound elastography had the potential of predicting lung malignancy with a suggested cut-off point [19]. Another study revealed that the strain ratio of different pulmonary lesions from low to high included necrosis, atelectasis, consolidation, and tumor [20]. In addition, ultrasound elastography was considered a feasible technique for classifying mediastinal lymph nodes, especially in combination with conventional endobronchial ultrasound imaging [21]. Our current study demonstrated by vMRE that malignant neoplasms were significantly stiffer than benign ones. These results are consistent with prior work on ultrasound elastography.

The reason for this observation may be that increased stiffness of cancer is caused by matrix deposition and remodeling, which can activate signaling pathways that promote proliferation, invasiveness, and metastasis [3, 22]. When normal tissue architecture is disrupted by cancer growth and invasion, microarchitecture is altered [23]. Increased deposition and cross-linking of the extracellular matrix (ECM) lead to matrix stiffening. Increased ECM stiffness and TGF-β signaling activate fibroblasts to become cancer-associated fibroblasts (CAF), initiating a positive feedback loop that further enhances ECM stiffening [24, 25]. Additionally, some collagen fibers are under tension due to cell contraction or local expansion caused by tumor growth [26]. These tensile stresses increase the stiffness of the collagen network, which in turn further activates the focal adhesion contractility of the CAFs in their vicinity, leading to a vicious cycle of matrix deposition and stiffening [27].

Hence, vMRE method may potentially provide a better understanding of microstructural tissue changes in pulmonary neoplasm and enable fast and detailed evaluation of tumor stiffness. Subsequent subtype analyses showed both sADC and virtual stiffness values of adenocarcinoma and squamous cell carcinoma groups were significantly different from non-specific benign group. However, no significant correlation was found in small cell carcinoma and tuberculosis groups. As small cell carcinoma has a faster proliferation rate and reduced extracellular space compared to non-small cell lung cancer, which results in a significant reduction of water diffusion in the tumor, it should theoretically present a higher stiffness. Our negative result regarding small cell carcinoma and tuberculosis may have been due to the small sample size.

There are certain intrinsic limitations to our study. The sample size of the study was not big enough. Therefore, we performed G*power to assess the power of our study. The α vaule was set as 0.05, and the calculated 1-β value of sADC and mean virtual stiffness value between malignant and benign groups were 0.996 and 0.842, respectively. Even so, we believe future studies should include larger samples than the small size used here. Moreover, MR lung imaging has limitations. Although the nonrigid registration reduces artifacts caused by motion displacement to a certain extent, it is still difficult to eliminate the influence of respiratory motion. Additionally, objects that change the magnetic field such as calcification may cause certain inaccuracy due to the principle of IVIM-based virtual elastography calculation. Therefore, it follows that the pulmonary neoplasms of the excluded cases are mostly located in the lower lung lobes, where respiratory motion is accentuated.

Conclusions
In conclusion, our findings provide evidence that malignant neoplasms have significantly lower sADC and higher mean virtual stiffness values than benign ones. There is efficacy in the pathological diagnosis that adenocarcinoma and squamous cell carcinoma are stiffer than non-specific benign neoplasm. To our knowledge, this is the first report of IVIM-based virtual elastography used for pulmonary neoplasm as a promising alternative to invasive biopsy and routine MRE.

Abbreviations

IVIM	Intravoxel incoherent motion
vMRE	Virtual magnetic resonance elastography
sADC	Shifted apparent diffusion coefficient
PTNB	Percutaneous transthoracic needle biopsy
MRE	Magnetic resonance elastography
ROI	Regions of interest
ROC	Receiver operating characteristic
ICC	Intraclass correlation coefficients
FIESTA	T1-weighted fast imaging employing steady-state acquisition
FSE	Fat saturated T2-weighted fast spin echo
DWI	Diffusion-weighted imaging
D	Diffusivity
ADC	Apparent diffusion coefficient
f	Perfusion fraction
D*	Pseudo-diffusivity
NGD	Non-Gaussian diffusion index
ECM	Extracellular matrix
CAFs	Cancer-associated fibroblasts

Author contributions
All authors contributed to the study conception and design. Material preparation, data collection and analysis were performed by Shuo Zhang, Yonghao Du, Ting Liang and Yinxia Guo. Statistical analysis was performed by Xuyin Zhang. MATLAB procedure for vMRE stiffness quantification were designed by Xianjun Li and Jian Yang. Resources, project administration and supervision was by Gang Niu. Manuscript was written by Shuo Zhang. Gang

Zhang et al. Cancer Imaging   (2024) 24:88

Page 8 of 8

Niu and all authors commented on previous versions of the manuscript. All authors read and approved the fnal manuscript.

Declarations

Ethics approval and consent to participate
This study was approved by the Institutional Review Boards of Xi'an Jiaotong University (No. 2021 − 146). Written informed consent was obtained for all participants. The related clinical data of the patients were collected using face-to-face questionnaires and medical case records. All patients were informed of the MRI contraindications.

Consent for publication
Not applicable.

Competing interests
All authors declare no competing interests.

References

1. Chen W, Zheng R, Baade PD, Zhang S, Zeng H, Bray F, Jemal A, Yu XQ, He J. Cancer statistics in China, 2015. CA Cancer J Clin. 2016;66(2):115–32.
2. Siegel RL, Miller KD, Fuchs HE, Jemal A. Cancer statistics, 2021. CA Cancer J Clin. 2021;71(1):7–33.
3. Nia HT, Munn LL, Jain RK. Physical traits of cancer. Science 2020, 370(6516).
4. McGee KP. Virtual palpation: the role of MR Elastography in quantifying and spatially resolving tissue stiffness as a biomarker of Disease. J Am Coll Radiol. 2018;15(5):778–80.
5. Le Bihan D, Ichikawa S, Motosugi U. Diffusion and Intravoxel Incoherent Motion MR Imaging-based virtual elastography: a hypothesis-generating study in the liver. Radiology. 2017;285(2):609–19.
6. Kromrey ML, Le Bihan D, Ichikawa S, Motosugi U. Diffusion-weighted MRI-based virtual elastography for the Assessment of Liver Fibrosis. Radiology. 2020;295(1):127–35.
7. Ota T, Hori M, Le Bihan D, Fukui H, Onishi H, Nakamoto A, Tsuboyama T, Tatsumi M, Ogawa K, Tomiyama N. Diffusion-based virtual MR Elastography of the liver: can it be extended beyond liver fibrosis? J Clin Med 2021, 10(19).
8. Hanniman E, Costa AF, Bowen CV, Abdolell M, Stueck A, McLeod M, Peltekian K, Rioux J, Clarke SE. Prospective evaluation of virtual MR Elastography with Diffusion-Weighted imaging in subjects with nonalcoholic fatty liver disease. J Magn Reson Imaging. 2022;56(5):1448–56.
9. Lagerstrand K, Gaedes N, Eriksson S, Farahmand D, De Coursey E, Johansson G, Jonsson L, Skoglund T. Virtual magnetic resonance elastography has the feasibility to evaluate preoperative pituitary adenoma consistency. Pituitary. 2021;24(4):530–41.
10. Aunan-Diop JS, Andersen MCS, Friismose AI, Halle B, Pedersen CB, Mussmann B, Gronhoj MH, Nielsen TH, Jensen U, Poulsen FR. Virtual magnetic resonance elastography predicts the intraoperative consistency of meningiomas. J Neuroradiol 2022.
11. Alkalay RN, Burstein D, Westin CF, Meier D, Hackney DB. MR diffusion is sensitive to mechanical loading in human intervertebral disks ex vivo. J Magn Reson Imaging. 2015;41(3):654–64.
12. Lee KH, Lim KY, Suh YJ, Hur J, Han DH, Kang MJ, Choo JY, Kim C, Kim JI, Yoon SH, et al. Nondiagnostic percutaneous transthoracic needle biopsy of lung lesions: a Multicenter Study of Malignancy Risk. Radiology. 2019;290(3):814–23.
13. Liang J, Li J, Li Z, Meng T, Chen J, Ma W, Chen S, Li X, Wu Y, He N. Differentiating the lung lesions using Intravoxel incoherent motion diffusion-weighted imaging: a meta-analysis. BMC Cancer. 2020;20(1):799.
14. Zheng Y, Huang W, Zhang X, Lu C, Fu C, Li S, Lin G. A Noninvasive Assessment of Tumor Proliferation in Lung cancer patients using Intravoxel Incoherent Motion magnetic resonance imaging. J Cancer. 2021;12(1):190–7.
15. Jiang J, Fu Y, Hu X, Cui L, Hong Q, Gu X, Yin J, Cai R, Xu G. The value of diffusion-weighted imaging based on monoexponential and biexponential models for the diagnosis of benign and malignant lung nodules and masses. Br J Radiol. 2020;93(1110):20190400.
16. Shi C, Liu D, Xiao Z, Zhang D, Liu G, Liu G, Chen H, Luo L. Monitoring tumor response to Antivascular Therapy using Non-contrast Intravoxel Incoherent Motion Diffusion-Weighted MRI. Cancer Res. 2017;77(13):3491–501.
17. Huang C, Liang J, Ma M, Cheng Q, Xu X, Zhang D, Shi C, Shang N, Xiao Z, Luo L. Evaluating the treatment efficacy of Nano-Drug in a Lung Cancer Model using Advanced Functional magnetic resonance imaging. Front Oncol. 2020;10:563932.
18. Iima M, Le Bihan D. Clinical Intravoxel Incoherent Motion and Diffusion MR Imaging: past, Present, and Future. Radiology. 2016;278(1):13–32.
19. Kuo YW, Chen YL, Wu HD, Chien YC, Huang CK, Wang HC. Application of transthoracic shear-wave ultrasound elastography in lung lesions. Eur Respir J 2021, 57(3).
20. Lim CK, Chung CL, Lin YT, Chang CH, Lai YC, Wang HC, Yu CJ. Transthoracic Ultrasound Elastography in Pulmonary lesions and diseases. Ultrasound Med Biol. 2017;43(1):145–52.
21. Gu Y, Shi H, Su C, Chen X, Zhang S, Li W, Wu F, Gao G, Wang H, Chu H, et al. The role of endobronchial ultrasound elastography in the diagnosis of mediastinal and hilar lymph nodes. Oncotarget. 2017;8(51):89194–202.
22. Guo H, Zhang T, Yu Y, Xu F. Cancer Physical Hallmarks as new targets for Improved Immunotherapy. Trends Cell Biol. 2021;31(7):520–4.
23. Le Bihan D. What can we see with IVIM MRI? NeuroImage. 2019;187:56–67.
24. Lee J, Condello S, Yakubov B, Emerson R, Caperell-Grant A, Hitomi K, Xie J, Matei D. Tissue transglutaminase mediated Tumor-Stroma Interaction promotes pancreatic Cancer Progression. Clin Cancer Res. 2015;21(19):4482–93.
25. Li CX, Talele NP, Boo S, Koehler A, Knee-Walden E, Balestrini JL, Speight P, Kapus A, Hinz B. MicroRNA-21 preserves the fibrotic mechanical memory of mesenchymal stem cells. Nat Mater. 2017;16(3):379–89.
26. Samuel MS, Lopez JI, McGhee EJ, Croft DR, Strachan D, Timpson P, Munro J, Schroder E, Zhou J, Brunton VG, et al. Actomyosin-mediated cellular tension drives increased tissue stiffness and beta-catenin activation to induce epidermal hyperplasia and tumor growth. Cancer Cell. 2011;19(6):776–91.
27. Choquet D, Felsenfeld DP, Sheetz MP. Extracellular matrix rigidity causes strengthening of integrin-cytoskeleton linkages. Cell. 1997;88(1):39–48.

Publisher's Note